PSA-STT-MRAM solution for extended temperature stability

Steven Lequeux
INAC-SPINTEC
Univ. Grenoble Alpes, CEA, CNRS, Grenoble INP
Grenoble, France
steven.lequeux@cea.fr

Trevor Almeida
CEA Leti
Univ. Grenoble Alpes
Grenoble, France
trevor.almeida@cea.fr

Nuno Caçoilo
INAC-SPINTEC
Univ. Grenoble Alpes, CEA, CNRS, Grenoble INP
Grenoble, France
nuno.cacoilo@cea.fr

Alvaro Palomino
INAC-SPINTEC
Univ. Grenoble Alpes, CEA, CNRS, Grenoble INP
Grenoble, France
alvaro.palomino@cea.fr

Ioan Lucian Prejbeanu
INAC-SPINTEC
Univ. Grenoble Alpes, CEA, CNRS, Grenoble INP
Grenoble, France
ricardo.sousa@cea.fr

Ricardo C. Sousa
INAC-SPINTEC
Univ. Grenoble Alpes, CEA, CNRS, Grenoble INP
Grenoble, France
ricardo.sousa@cea.fr

David Cooper
CEA Leti
Univ. Grenoble Alpes
Grenoble, France
David.cooper@cea.fr

Bernard Dieny
INAC-SPINTEC
Univ. Grenoble Alpes, CEA, CNRS, Grenoble INP
Grenoble, France
bernard.dieny@cea

***Abstract*— The concept of Perpendicular Shape Anisotropy (PSA) spin transfer torque (STT) MRAM has been recently proposed as a solution to achieve downsize scalability of MRAM below sub-10 nm technology nodes, down to 3-4 nm cell size lateral dimensions. In conventional p-STT-MRAM, at sub-20 nm diameters, the perpendicular anisotropy arising from the MgO/CoFeB interface becomes too weak to ensure sufficient stability of the storage layer magnetization. In addition, this interfacial anisotropy decreases rapidly with increasing temperature, resulting in a significant drawback for applications having to operate on a wide temperature range. Here, we combine both coercivity and electron holography measurements as function of temperature to show that in a PSA storage layer, the source of anisotropy is much more robust versus temperature compared to the interfacial anisotropy of conventional STT-MRAM stacks. This allows to considerably reduce the temperature dependence of coercivity. This property is quite beneficial for applications having to operate on an extended temperature range, such as automotive (-40°C to 150°C), or to fulfill solder reflow compliance requiring 1 minute retention at 260°C.**

Keywords—Perpendicular Shape Anisotropy, STT-MRAM, MTJ, temperature sensitivity, Electron Holography.

I. INTRODUCTION

The interest in perpendicular spin transfer torque magnetic memories (p-STT-MRAM) has been increasing during the last decade because of their non-volatility, nanosecond read and write speeds, 1015 cycle endurance, low consumption and scaling properties [1]. P-STT-MRAM devices have replaced in-plane magnetized cells because of their better tradeoff between retention and writability [2], leading to an extensive effort towards the optimization of magnetic tunnel junctions (MTJ) exhibiting Perpendicular Magnetic Anisotropy (PMA) [3]. A key goal is to ensure data storage retention while minimizing the write power consumption of these devices. Cell retention is determined by the thermal stability factor Δ, where Δ=EbkB.T, with Eb the energy barrier between parallel (P) and anti-parallel (AP) configurations, kB is the Boltzmann constant, and T is the absolute temperature. One particular challenge of p-STT-MRAM is to decrease the diameter of the junctions below the 20 nm critical dimension, while maintaining a thermal stability factor Δ corresponding to the target retention time of stored data (for instance 10 years) [4]. It has been shown in conventional stacks that the stability of the storage layer magnetization becomes insufficient below 20 nm diameter cells [4]–[6]. The decrease of the thermal stability factor results from the reduction in the net perpendicular anisotropy existing at the MgO/CoFeB interface (iPMA). Indeed this net surface anisotropy scales proportionally to the cell area in the macrospin re This work was partly funded by the ERC advanced grant MAGICAL n°669204, the ERC Starting grant Holoview Nº306535 and the Carnot project MAGICMAPS.gime. This limits the downsize scalability of conventional STT-MRAM and their use at elevated operating temperature. A first solution has been proposed by introducing a second top FeCoB/MgO interface, but the difficulty to maintain a thermal stability factor of 60 at sub-20 nm diameters [7], [8] remains.

II. DEVICE DESCRIPTION

In order to combine extreme scalability in p-MTJs with high thermal stability factor, a promising solution has been proposed in the concept of perpendicular shape anisotropy STT-MRAM [9]–[11]. This concept relies on a dramatic increase of the thickness of the storage ferromagnetic (FM) layer compared to conventional STT-MRAM stack. While this thickness is typically ~1.4-2.5 nm in conventional stacks, in PSA-STT-MRAM, it is increased to values of the order of the cell diameter. The resulting storage layer aspect ratio ρ=t/D determines the cell stability, where t and D are respectively the layer thickness and cell diameter. This ratio must be close to 1 or higher, to induce a perpendicular shape anisotropy in the storage layer which comes on top of its interfacial PMA. This represents a strong and tunable source of bulk anisotropy, enabling a significantly increased downsize scalability. Another advantage of the large storage layer thickness is that its magnetization and anisotropy are much closer to bulk material properties than in conventional STT-MRAM. This means that they are expected to exhibit a

weaker temperature dependence compared to STT- MRAM devices based on iPMA.

Figure 1(a) shows a schematic representation of a PSA-STT-MRAM cell. The tunnel junction stack as the following composition: SiO_2/Pt (25)/SAF/Ta (0.3)/FeCoB (1.1)/MgO (1.2)/FeCoB (1.4)/W (0.2)/**FM** (t)/Ta (1)/Ru (10)/Ta (150) (thickness in nm), where the FM layer of thickness t corresponds to the thick storage layer deposited on top of the conventional reference layer stack [9]. In the case of Fig. 1, the FM storage electrode is a NiFe 60 nm thick layer. After nanofabrication, PSA cells were imaged by Scanning Transmission Electron Microscopy (STEM) using an FEI Titan Themis microscope operating at 200 kV. Fig. 1(b) shows a bright field micrograph of a first PSA pillar after the ion beam etch step, from which the physical diameter is estimated to be 17 nm at the storage layer mid-height. Figure 1(c) shows an elemental map of another PSA pillar obtained by energy dispersive X-ray spectroscopy (EDS), with a physical diameter that can be estimated to be 20 nm, at the NiFe storage layer mid-height. The nominal 60 nm height of the storage layer is confirmed in both figures.

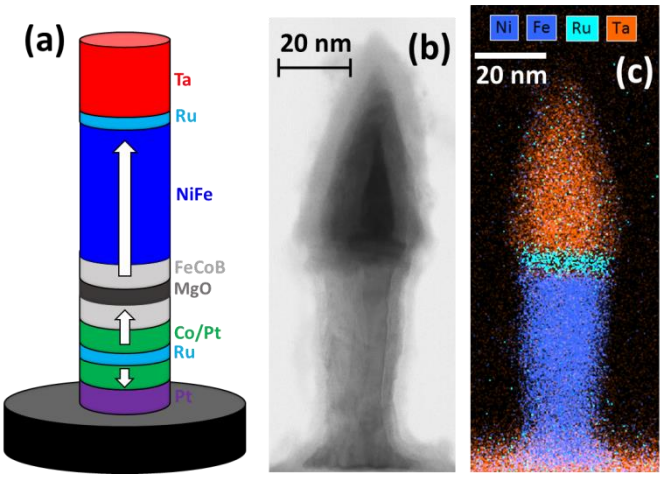

Fig. 1. (a) Schematic representation of a PSA-STT-MRAM MTJ cell with a storage layer comprising 60 nm of NiFe. The white arrows show the expected magnetic easy axis. (b) Bright field scanning transmission electron microscopy image of a first PSA pillar after the ion beam etching process, showing a diameter of 17 nm. (c) Element mapping using energy dispersive X-ray spectroscopy of a second pillar showing a diameter of 20 nm. Representations of each color are Ta: red, Ni/Fe: blue, Ru: Light blue.

III. Experimental Measurements

A. *Coercive field versus temperature measurement in 5nm diameter PSA-STT-MRAM cell*

In order to study the impact of temperature on the anisotropy of the PSA storage layer and the associated decrease of coercivity due to thermal activation, the coercive field Hc was measured as function of temperature. These measurements were done in a temperature range from 10 to 300 K, both on a 5 nm diameter PSA cell with 60 nm NiFe storage layer thickness, shown in Fig. 2 (a, c) and also on a conventional p-STT-MRAM cell in Fig. 2(b). The conventional p-MTJ has an FeCoB 1.5 nm/W 0.2 nm/ FeCoB 1.2 nm storage layer sandwiched between two MgO tunnel barriers with a diameter of 70 nm. The value of the diameter D is calculated based on the device electrical resistance in parallel (P) state based of the resistance area product, measured on continuous films from Current In Plane Tunneling measurements [12]. Figure 2 (a) shows the evolution of the normalized resistance as a function of a perpendicular applied field at 10, 100, 200 and 300 K. Figure 2 (b) shows the same measurement at 10 and 300 K. Fig. 2(c) shows the evolution of Hc for a 5 nm diameter PSA device as a function of the temperature in the full range [10-300] K. The coercivity of the device is still of 1.3kOe at RT, demonstrating the extreme downsize scalability of PSA-STT-MRAM.

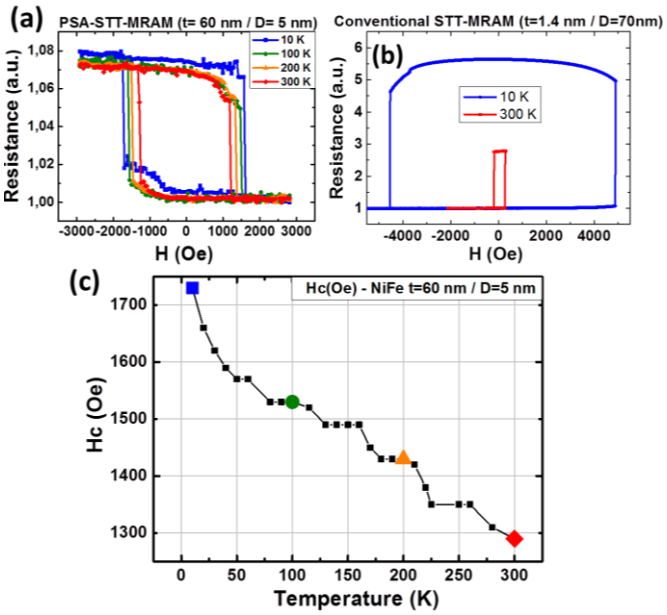

Fig. 2. (a) Normalized resistance versus perpendicular field measured at 10 K (blue square symbols), 100 K (green circle symbols), 200 K (orange triangle symbols) and 300 K (red diamond symbols), (b) normalized resistance versus perpendicular field measured at 10 K (blue square symbols) and 300 K (red diamond symbols) of a conventional STT-MRAM cell. (c) Evolution of the coercive field Hc with temperature in the range [10-300] K of a PSA MTJ cell comprising a 60 nm thick storage layer and an electrical diameter of 5 nm.

As expected, the loss of coercivity due to temperature is significantly higher for the conventional p-STT-MRAM (Fig. 2b), compared to the PSA cell type (Fig. 2a). The coercive field of the PSA device drops from 1730 Oe at 10 K to 1290 Oe at room temperature, i.e. a coercivity reduction by a factor of 1.34 over the 290 K temperature range. This compares to a coercive field reduction from 4565 to 345 Oe, from 10 K to 300 K, i.e. a factor 13 reduction, for the conventional MRAM stack. This represents a much higher temperature dependence of the conventional stack, almost 10 times higher compared to a PSA stack, as evaluated from the coercivity measurements.

B. *Storage Layer Coercivity vs Temperature: Thickness and Composition Dependence*

o extend the analysis of the temperature dependence, both coercivity and tunnel magneto resistance (TMR) ratio were measured as a function of temperature on a conventional junction stack and on three different PSA storage layer stacks. In figures 3 and 4, the FM material of the PSA stacks is either a 60 nm Co layer or a NiFe layer of thickness 30 or 60 nm. The data are plotted in figures 3–4 (b), with the same symbol correspondence. In each PSA stack, the normalized coercivity change δHc/Hc is reported in Fig. 3 using the average coercivity measured on two different samples from 10 K up to 380 K. Normalization uses the high temperature as reference, i.e. $\frac{\delta Hc(T)}{Hc} =$

$\frac{(Hc(T)-Hc(380K))}{Hc(380K)}$. For conventional p-STT-MRAM in Fig. 3(a), the coercive field is measured on a single sample in the same 10–300 K temperature interval, and the normalization reference is the measured value at 340 K.

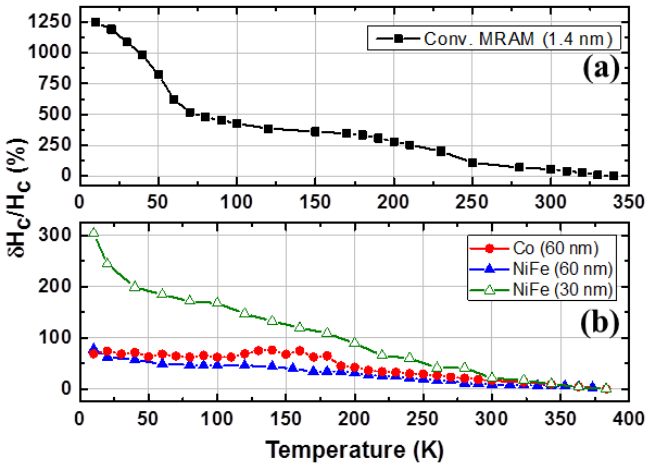

Fig. 3. (a) Thermal variation in the range [10, 340] K of the coercive field he normalized by its value at 340 K of a conventional p-STT-MRAM comprising a FeCoB 1.5 nm/W 0.2 nm/FeCoB 1.2 nm storage layer sandwiched between two mgo barriers. (b) Thermal variation in the range [10], [380] K of he normalized by its value at 380 K for three different PSA stacks: 60 nm thick co storage layer (red line), 60 nm thick NiFe storage layer (blue line) and 30 nm thick NiFe storage layer (green line). For each stack, the temperature dependence of Hc was measured on two samples and then averaged before normalization by the value of hc measured at 383 K.

In agreement with single device measurements from Fig. 2, the data in Fig. 3 clearly show the benefits of the PSA in terms of reduction of the temperature dependence of cell magnetic properties. This is reflected by a much weaker variation of the coercivity, over the whole temperature range from 10 K to 340 K. All PSA cell stacks show a reduced variation. In the thinner 30 nm NiFe PSA electrode, the variation amplitude is reduced by a factor 4 compared to the conventional MRAM cell. For thicker 60 nm PSA electrodes, consisting of either NiFe or Co, further reduction of the variations are observed to about 70% for both Co and NiFe. This trend is also conserved around room temperature. For the conventional stack, the relative decrease of coercivity per degres is 1.45%/K while for the PSA stacks, it is only 0.12%K, 0.19%/K and 0.26%/K, respectively for 60 nm Co, 60 nm NiFe and 30 nm NiFe electrodes. The smallest coercivity loss of the Co based storage layer can be explained by the higher Curie temperature value of Co, Tc_Co=1388 K, compared to that of NiFe, Tc_NiFe=826 K [13],[14]. This is due to the fact that the shape anisotropy is proportional to the square of the saturation magnetization Ms2. The consequence of a higher Curie temperature is a slower decrease of Ms with temperature, resulting in a weaker thermal variation of the shape anisotropy compared to surface anisotropy of conventional p-MTJs [15].

C. TMR vs Temperature: Storage Layer Thickness and Composition Dependence

As was already evident from TMR loops in Fig. 2, there is also a significant temperature dependence of the TMR ratio. It is well known that thermal activation in tunnel junction yields a weak decrease of the junction resistance versus temperature in the parallel magnetic configuration. Besides, as the temperature increases, there is a reduction of the spin polarization due to interfacial magnetic fluctuations yielding a stronger decrease of the junction resistance in antiparallel configuration [16]. The temperature dependence of the TMR ratio for conventional and PSA MTJs is shown in Fig. 4, plotting the normalized TMR change as:

$\frac{\delta TMR(T)}{TMR} = \frac{(TMR(T)-TMR(380K))}{TMR(380K)}$).

A weaker decrease of TMR versus temperature is observed in the PSA MTJ than in the conventional MTJ. However, the difference is not as pronounced as in the case of the coercivity variation. This difference between coercivity variation and TMR variation originates from the fact that the coercivity is quite influenced by the bulk properties of the storage layer whereas the TMR remains mostly an interfacial effect. The fact that the conventional p-MTJ still exhibits a larger TMR decrease than the PSA-MTJs can be ascribed to the higher density of thermal fluctuations along the MgO interface in the former case than in the latter.

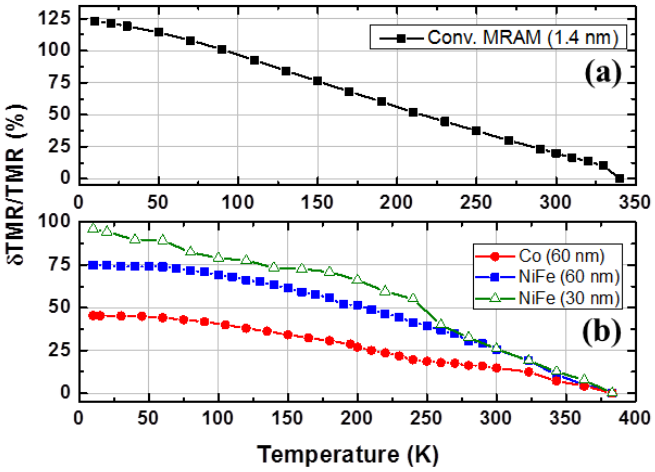

Fig. 4. ((a) Thermal variation in the range [10, 340] K of the TMR ratio normalized by its value at 340 K for a conventional p-STT-MRAM storage layer: FeCoB 1.5 nm/W 0.2 nm/FeCoB 1.2 nm sandwiched between two MgO barriers. (b) Thermal variation in the range [10, 380] K of the averaged TMR ratio normalized by its value at 380 K of three PSA stacks: 60 nm thick Co storage layer (red line), 60 nm thick NiFe storage layer (blue line) and 30 nm thick NiFe storage layer (green line). For each stack, the temperature dependence of the TMR ratio was measured on two samples and then averaged before normalization by the value of TMR measured at 383 K.

Between the three PSA stacks, the ones with NiFe electrodes exhibit higher TMR drops: 96 and 75%, respectively for 30 and 60 nm thick electrodes, compared to 45% for Co electrode. Due to exchange interaction, a magnetic stiffening of the magnetization along the MgO/storage layer interface can be expected when a thick storage layer is used especially for a high Curie temperature material such as cobalt.

IV. Electron Holography Measurements

To further investigate the stability of the magnetization of PSA-STT-MRAM device versus temperature, electron holography measurements were performed at temperatures between 25 and 250°C. Such holography measurements allow reconstruction of the magnetic induction map of a magnetic sample, from which the direction of the magnetic field lines can be deduced [17]–[19].

Figure 5 shows electron holography measurements for a PSA device having a 60 nm thick NiFe storage layer and a diameter of 18 nm at pillar mid-height. The color map corresponds to magnetic field lines where the color of the

lines depicts the orientation of the field, according to the arrow directions on the color wheel.

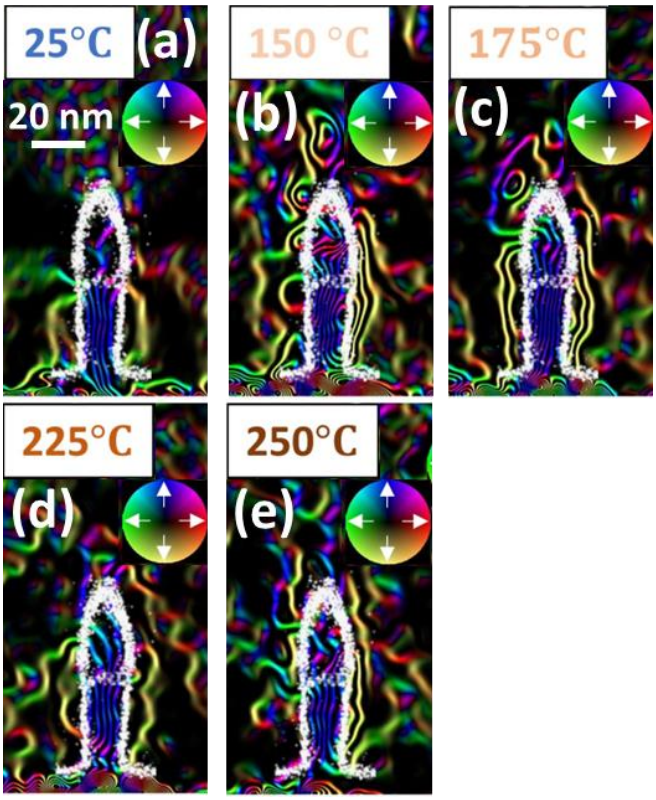

Fig. 5. Results of electron holography measurements showing a color map of the magnetic field lines orientation according to the color wheel direction arrows at various temperature: (a) 25°c, (b) 150°c, (c) 175°c, (d) 225°c and (e) 250°c. The thick white line corresponds to the contour of the PSA pillar having a 60 nm thick storage of NiFe and a diameter of 18 nm. The constant figure scale is shown on (a).

Thick white line represents the pillar contours, which can be related to Fig. 1(b, c) such that the pillar base section corresponds to the 60 nm thick NiFe storage layer and the top part corresponds to the non-magnetic Ta hardmask. The vertical blue lines within the storage layer on Fig. 5(a) show the magnetization of the storage layer pointing vertically along the height of the pillar, as expected for PSA cells. When the temperature increases up to 250°C, no changes is observed in the blue magnetic field lines. This demonstrates that even at 250°C, the magnetization of the PSA MTJ remains aligned along the pillar vertical axis, the perpendicular shape anisotropy of this high aspect ratio pillar is still effective.

V. CONCLUSIONS

In this paper, the temperature dependence of the magnetic and electrical properties of PSA-STT-MRAM devices with different storage layer thicknesses and composition have been investigated. The evolution of the coercive field with temperature was compared with that of conventional STT-MRAM stack. This comparison shows that perpendicular shape anisotropy provided by a thick storage layer yields a much stronger thermal robustness of the coercivity in PSA-MTJ cells compared to conventional p-MTJ cells. Indeed, the bulk perpendicular shape anisotropy of a vertically elongated storage layer provides a more robust source of anisotropy than the surface anisotropy at the MgO/CoFeB interface. Both coercive field and electron holography measurements show that PSA is stable over a wide range of temperatures, from 10 K up to 525 K. In addition, the density of thermal fluctuations along the MgO/CoFeB interface at increasing temperature is reduced by magnetic stiffening associated with the use of thicker storage layers from high Curie temperature materials. This yields a weaker thermal variation of the TMR ratio compared to conventional p-STT-MRAM devices. In terms of applications, this robustness of magnetic and transport properties against thermal variations is necessary to enable operation on a wide range of temperatures, e.g. automotive −40°C to +150°C, or to fulfill solder reflow compliance requirements.

ACKNOWLEDGEMENTS

This work was partly funded by the ERC advanced grant MAGICAL n°669204, the ERC Starting grant Holoview Nº306535 and the Carnot project MAGICMAPS.

REFERENCES

[1] S. Ikeda, K. Miura, H. Yamamoto, K. Mizunuma, H. D. Gan, M. Endo, S. Kanai, J. Hayakawa, F. Matsukura, and H. Ohno, Nature Materials 9, 721 (2010).

[2] S. Mangin, D. Ravelosona, J. A. Katine, M. J. Carey, B. D. Terris and E. E. Fullerton, Nat. Mater., 2006, 5, 210–215.

[3] B. Carvello, C. Ducruet, B. Rodmacq, S. Auffret, E. Gautier, G. Gaudin and B. Dieny, Appl. Phys. Lett., 2008, 92, 102508.

[4] H. Sato, E. C. I. Enobio, M. Yamanouchi, S. Ikeda, S. Fukami, S. Kanai, F. Matsukura and H. Ohno, Appl. Phys. Lett., 2014, 105, 062403.

[5] L. Thomas, G. Jan, J. Zhu, H. Liu, Y.-J. Lee, S. Le, R.-Y. Tong, K. Pi, Y.-J. Wang, D. Shen, R. He, J. Haq, J. Teng, V. Lam, K. Huang, T. Zhong, T. Torng and P.-K. Wang, J. Appl. Phys., 2014, 115, 172615.

[6] H. Sato, S. Ikeda and H. Ohno, Jpn. J. Appl. Phys., 2017, 56, 0802A6.

[7] H. Sato, M. Yamanouchi, S. Ikeda, S. Fukami, F. Matsukura and H. Ohno, IEEE Trans. Magn., 2013, 49, 4437–4440.

[8] G. Jan, Y.-J. Wang, T. Moriyama, Y.-J. Lee, M. Lin, T. Zhong, R.-Y. Tong, T. Torng and P.-K. Wang, Appl. Phys. Express, 2012, 5, 093008.

[9] N. Perrissin, S. Lequeux, N. Strelkov, A. Chavent, L. Vila, L. D. Buda-Prejbeanu, S. Auffret, R. C. Sousa, I. L. Prejbeanu and B. Dieny, Nanoscale, 2018, 10, 12187–12195.

[10] K. Watanabe, B. Jinnai, S. Fukami, H. Sato and H. Ohno, Nat. Commun., 2018, 9, 663.

[11] S. Lequeux, N. Perrissin, G. Grégoire, L. Tillie, A. Chavent, N. Strelkov, L. Vila, L. D. Buda-Prejbeanu, S. Auffret, R. C. Sousa, I. L. Prejbeanu and B. Dieny, Nanoscale, 2020,12, 6378-6384.

[12] A. Cagliani, F. W. Østerberg, O. Hansen, L. Shiv, P. F. Nielsen and D. H. Petersen, Rev. Sci. Instrum., 2017, 88, 095005.

[13] K.-M. Lee, J. W. Choi, J. Sok and B.-C. Min, AIP Adv., 2017, 7, 065107.

[14] S. Yuasa, A. Fukushima, H. Kubota, Y. Suzuki and K. Ando, Appl. Phys. Lett., 2006, 89, 042505.

[15] L. J. M. Iwata-Harms, G. Jan, H. Liu, S. Serrano-Guisan, J. Zhu, L. Thomas, R.-Y. Tong, V. Sundar and P.-K. Wang, Sci. Rep., 2018, 8, 14409.

[16] J. H. van Vleck, Phys. Rev., 1937, 52, 1178–1198.

[17] L. A. Tonomura, T. Matsuda, J. Endo, T. Arii and K. Mihama, Phys. Rev. Lett., 1980, 45, 1430.

[18] R.E. Dunin-Borkowski, T. Kasama, A. Wei, S.L. Tripp, M. J. Hÿtch, E. Snoeck, R.J. Harrison and A. Putnis, Microsc. Res. Tech., 2004, 64, 390–402.

[19] V. Boureau, V. D. Nguyen, A. Masseboeuf, A. Palomino, E. Gautier, J. Chatterjee, S. Lequeux, S. Auffret, L. Vila, R. Sousa, L. Prejbeanu, D. Coopera and B. Dieny, Nanoscale, 2020,12, 17312-173.